applied sciences

MDPI

Article

The San Giovanni Baptistery in Florence (Italy): Assessment of the State of Conservation of Surfaces and Characterization of Stone Materials

Sara Calandra [1,2], Emma Cantisani [3], Silvia Vettori [3,*], Marilena Ricci [2], Beatrice Agostini [4] and Carlo Alberto Garzonio [1]

[1] Department of Earth Sciences, University of Florence, 50121 Florence, Italy; sara.calandra@unifi.it (S.C.); carloalberto.garzonio@unifi.it (C.A.G.)
[2] Chemical Department "Ugo Schiff", University of Florence, Via della Lastruccia 3-13, Sesto Fiorentino, 50019 Florence, Italy; marilena.ricci@unifi.it
[3] Institute of Heritage Science, National Research Council of Italy, Via Madonna del Piano 10, Sesto Fiorentino, 50019 Florence, Italy; emma.cantisani@cnr.it
[4] Opera del Duomo di Firenze, 50212 Florence, Italy; b.agostini@duomo.firenze.it
* Correspondence: silvia.vettori@cnr.it

Abstract: During the last restoration campaign of the Baptistery of San Giovanni in Florence (Italy), the assessment of the state of conservation of external surfaces was performed, with a multi-analytical approach, in order to support the conservation and restoration treatments. Black crusts, red staining, sulphation, and organic patinas were identified. Moreover, a complete characterization of marble cladding, bricks, and mortars was carried out. A geochemical and minero-petrographic approach was used in order to classify and assess the provenance of marbles, and define raw materials and technologies of the production for bricks and mortars. Provenances from Italy (Carrara and Lasa marbles) and from Greece (Hymettus and Pentelicum marbles) were identified and attributed to different construction phases, restoration interventions, and re-use of ancient materials. For mortars, the obtained data suggested the use of local materials and traditional technologies for the production. Overall, two different minero-petrographic typologies were identified for the analyzed bricks.

Keywords: San Giovanni Baptistery; Florence; decay and alteration phenomena; marbles; mortars; bricks

Citation: Calandra, S.; Cantisani, E.; Vettori, S.; Ricci, M.; Agostini, B.; Garzonio, C.A. The San Giovanni Baptistery in Florence (Italy): Assessment of the State of Conservation of Surfaces and Characterization of Stone Materials. *Appl. Sci.* **2022**, *12*, 4050. https://doi.org/10.3390/app12084050

Academic Editor: Asterios Bakolas

Received: 21 February 2022
Accepted: 14 April 2022
Published: 16 April 2022

1. Introduction

The Baptistery of San Giovanni, one of the most ancient churches in Florence (Italy), and protected by UNESCO since 1982, sits opposite the city's cathedral, the church of Santa Maria del Fiore. Octagonal in plan, it is completely clad in slabs of white and green marble, according to the Tuscan dichromic (Figure 1). Raised on the foundations of a Roman building, it is a characteristic example of the Tuscan Romanesque style, dating from around the 11th century (it was consecrated in 1059) [1–4]. In the early 13th century, the apse was changed from circular to square; the roof was renewed in the 15th century. It is covered by a dome of eight segments resting on perimetral walls, but the dome cannot be detected from the outside because it is concealed by the walls which are raised above the arcade on the second level and crowned by a flattened pyramidal roof. Its maintenance is managed by the Opera di Santa Maria del Fiore (OPA), a private institution established in 1296.

Every conservation project should be based on a sound knowledge of the "object" to be conserved, both from a historical and artistic viewpoint, and from the characteristics of its constituent materials, production technique, and decay conditions [5].

During the last restoration campaign, between March 2014 and September 2015, considering the complexity and heterogeneity of the centuries-old architectural and artistic

stratifications of the Baptistery, the OPA promoted a great opportunity for integrated multidisciplinary research and studies to achieve a fuller historical and scientific knowledge about the stone materials used in the Florence Baptistery.

Figure 1. San Giovanni Baptistery in Florence (photo taken from the terrace of the Santa Maria del Fiore Cathedral).

This paper focuses on the characterization of cladding marbles, masonry materials (mortars and bricks), and on the study of their state of conservation. Different kinds of materials (white and veined marbles, mortars, bricks) were analyzed, often belonging to different constructive phases, with the purpose being not only to obtain a complete knowledge of the material, but also to identify the provenance, raw materials, and technologies of production.

The provenancing of white marbles, especially Mediterranean ones, is of great interest for archaeologists and art historians, but it is also one of the most debated problems of petroarchaeometry [6]. In recent years, it has been demonstrated that the application of minero-petrographic and geochemical methods, along with the comparison of data

with dataset obtained from quarry samples, allows us to suggest the provenance of white marbles [6–8].

In the case of marble slabs of the Baptistery, the research is aimed at identifying reused ancient marbles, the original ones used, and the more recent substitutions.

For the cladding materials, specific research on the main phenomena of alteration/decay and on the presence of traces of previous restoration interventions was carried out in order to address the restoration procedures.

In previous studies, other stone materials were identified, coming from the spolia of Roman ruins in Florence or Fiesole (Porfido Verde Antico, Porfido Rosso Antico, Breccia Greca Antica, Syenite) [9]. Local stones, such as serpentinites (verde Prato) and red marly limestones ("marmi" rossi), were identified and characterized in other Florentine monuments [10–13].

The paper presents a description of all sampled materials and of the chemical, mineralogical, and petrographic techniques, including optical microscopy (OM), X-ray powder diffraction (XRPD), Fourier-transform infrared spectroscopy (FTIR), thermogravimetric analysis (TGA), micro-Raman, and ^{13}C and ^{18}O isotopic analyzes used to gain a better understanding and characterization of the present materials, as well as their provenance and state of conservation. The results consist of, first of all, an evaluation of the main decay phenomena that affect especially white marble surfaces, an assessment of provenance of white and veined marbles, and a characterization of mortars and bricks.

2. Materials and Methods

During the restoration survey, several powders and micro fragments of 2 cm in size sampled by a scalpel, representative of the different materials (white and veined marbles, bricks, mortars) belonging to different sides of the Baptistery and Lantern, were collected (Figure 2). Figure 2 shows the plan of the Baptistery, and the numbering of the sides assigned during the sampling campaign. Table 1 summarizes the information about the collected samples and the characterization project.

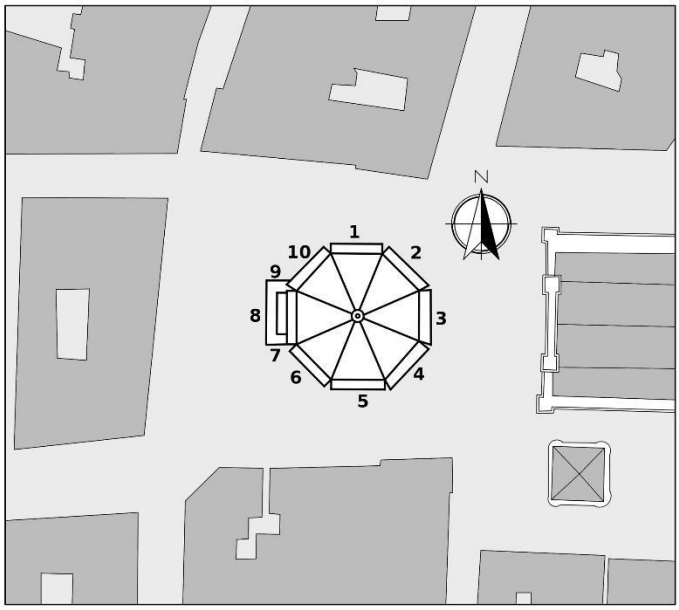

Figure 2. The octagonal plan of San Giovanni Baptistery in Florence. The numbering of the sides is reported.

Table 1. List of the collected stone materials samples, their localization on the monument, and the analytical methodologies applied in the investigation.

Type of Materials	Samples Number	Type of Analyzes	Position	Notes
Patina, encrustations, and other decay phenomena	25	XRPD, FT-IR, OM, Raman	sides 1, 3, 5, 6, 8, 9, 10	for the evaluation of the state of conservation and the identification of past treatments
White and veined marbles	27	XRPD, OM, C and O Isotopes	side 2 (5 samples) side 3 (2 samples) side 4 (5 samples) side 6 (9 samples) side 7 (2 samples) side 8 (1 sample) side 9 (2 samples)	for provenance assessment
Mortars	17 (core samples)	XRPD, OM, TGA	side 1 (1 core samples) side 4 (2 core sample) side 10 (2 core samples) basements (12 core samples)	for identification of raw materials and technologies of production
Bricks	4	XRPD, OM	side 4	for identification of differences related to different size and dating

XRPD = X-ray powder diffraction; OM = optical microscopy; TGA = thermo-gravimetric analysis; FT-IR = Fourier-transform infrared spectroscopy.

A total of 25 samples of patina and encrustations were investigated in order to characterise the state of conservation and the presence of previous treatments to best address the current restoration campaign; 27 microsamples of marbles were collected from different external sides, on the basis of macroscopic differences, and for the identification of the provenance; 17 core samples of mortars were gathered, from the Attic above the Matroneo, from the external and the internal walls, and from the foundations, at different depths, in relation to the different construction phases, and in order to establish the raw materials and the technologies used; 4 samples of bricks, representative of different sizes, were sampled from side 4. The selection of analyzed bricks was guided by different dates obtained with thermoluminescence technique [14].

All of the samples were first observed under a Zeiss stereomicroscope Stemi 200 C model, with a dedicated camera, and then fragments from each sample were divided and treated according to the protocol described in each technique used for investigating the sample characteristics.

Thin and cross sections were obtained by embedding the sample in epoxy resin (Epofix). In general, cross sections were observed with the optical microscope under reflected light under different magnifications, according to the available microscopy objectives. In this case, a Nikon Eclipse E600 optical microscope was used. Oriented thin sections (30 µm thick) were observed in transmitted light with a ZEISS Axioscope A1 microscope at different magnifications. The image analysis software Axiovision was used for the morphological and morphometric observation, for the evaluation of binder/aggregate ratio in the case of mortars [15–17], and of groundmass/ framework for bricks [18]. In the case of marbles, the petrographic observation allowed for the identification of MGS (maximum grain size), the fabric type (homeoblastic or heteroblastic), the main features of microstructure, and the crystal boundaries shapes, identified as the most relevant petrographic parameters for provenance determination [6,8]. For mortars, the petrographic approach allowed for a complete characterization of each component (binder, aggregate, and inorganic additives), as well as the identification of raw materials and technologies used for their production [17,19,20]. In the case of bricks, the optical characteristics of groundmass, the

presence and composition of framework, and the quantification of macroporosity could be obtained [21,22]. Optical microscopy was used also for the definition of macroporosity and the characterization of morphological aspects of black crusts and patinas.

X-ray powder diffractometry (XRPD) was employed to determine the mineralogical composition using a powder X-ray diffractometer (Cu anticathode (k = 1.54 Å)), under the following conditions: current intensity of 30 mA, voltage 40 kV, explored 2 h range between 3 and 70°, step size 0.02°, and time to step 50 s. The XRPD analyzes were performed on bulk samples of mortars, bricks, marbles, black crusts, and patinas.

Isotopic analyzes ($\delta^{13}C$, $\delta^{18}O$) were carried out on powders of marbles using a mass spectrometer (Finnigan MAT Delta Plus) equipped with Finnigan Gas-Bench II. Sample and standard mineral powders were treated with phosphoric acid for 1 h in sealed glass containers previously flushed with helium. The CO_2 produced was introduced into the mass spectrometer in continuous flow mode, using helium as carrier. The gas from the sample was run along the with reference CO_2 gas of a known composition. The experimental values were normalized against international (NBS-18) and internal standards. The mean external reproducibility was better than 0.1 for $\delta^{13}C$ and $\delta^{18}O$.

Fourier-transform infrared spectroscopy (FT-IR) was performed for the determination of patina and encrustations through a spectrometer Alpha Bruker. The acquisition of spectra was carried out directly on site by using the instrument equipped with the external total reflectance module for a contactless acquisition and a video camera. Spectra were collected in the range of 7000–400 cm^{-1} at a resolution of 4 cm^{-1} and 128 scans in order to optimise the signal-to-noise ratio, on a 4 mm diameter area. FT-IR analysis of powders were conducted, instead, with the ATR (attenuated total reflectance) configuration. The acquisition was carried out in the spectral range between 4000 and 400 cm^{-1}, with a resolution of 4 cm^{-1} for 24 scans. All of the acquired spectra were elaborated using the OPUS 7.2 software by Bruker.

A micro-chemical analysis of red and yellow patinas was carried out with a Renishaw single-grating (1200 grooves/mm) RM2000 micro-Raman spectrometer and charge-coupled device (CCD) air-cooled (577 × 400 pixels) detector. Spectra were recorded using a near infrared diode laser (785 nm) employed as an excitation source. Laser beam focusing was accomplished through a 50× magnification objective that provided a 1.5 μm laser spot diameter. Neutral density filters were used to attenuate the laser power in order to avoid phase transformations. The laser power at the analyzed samples was within the range 1–2 mW. The spectral range investigated was between 200 and 2000 cm^{-1}. Acquisition times were in the order of 30 s, and the spectral resolution was 4 cm^{-1} for the diode laser.

Thermo-gravimetric analysis (TGA) was employed for binder characterization of mortars. Some fragments of each sample were disaggregated using a porcelain pestle, and the fraction passing through a sieve with 63 μm openings (ISO R 565 Series) was considered as a binder-enriched specimen. TGA was used to evaluate the presence and the amount of particular volatile compounds (essentially H_2O, CO_2) in the samples. TGA was conducted in the range 110–1000 °C on approximately 5 mg of sample, and dried (silica gel as drying agent) at room temperature for at least a week under the following experimental conditions: open alumina crucibles, heating rate of 10 °C/min, and 30 mL/min nitrogen gas flow. TGA was used for classifying the studied samples as hydraulic or non-hydraulic mortars, as suggested by most authors [23–25]. TGA analyzes were performed using a Perkin Elmer Pyris 6 system on mortar samples.

A list of different types of materials analyzed and of methodologies applied for each material are reported in Table 1.

3. Results and Discussion

3.1. Evaluation of the State of Conservation: Main Decay Phenomena

An important aspect has been the technical–scientific support to the restoration interventions, mainly aimed at cleaning, through the diagnosis of the altering processes of the materials of the external cladding of the San Giovanni Baptistery, especially white marble.

In Table S1, the main results of state of conservation of external sides of San Giovanni Baptistery (Florence) are reported.

Many capitals, cornices, and decorated cornices of the windows and columns, beyond the intensity of the black crusts or deposits of dirt, were often affected by various decay phenomena, not only chemical–physical (e.g., sulfation), but also physical–mechanical (e.g., abrasion, decohesion, granular disintegration, with potential displacement and detachment, and differences in macro and micro porosity) (Figures 3 and 4).

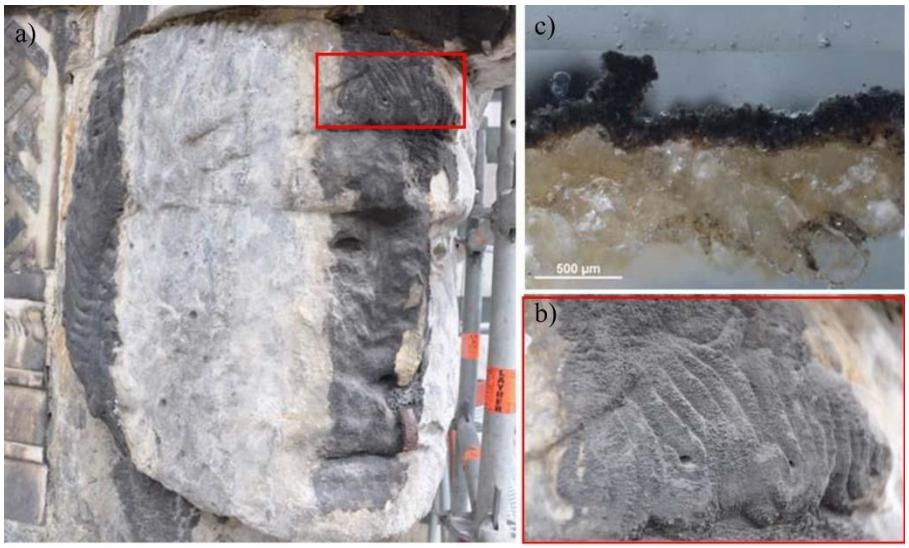

Figure 3. Scarsella, south corner. (**a**) Angular-shaped human head in marble: loss of molded and black crusts; (**b**) a detail of the black crust (red square); (**c**) a cross section of a micro fragment of a black crust.

Figure 4. (**a**) An example of a widespread granular disintegration phenomenon (see detail in (**b**)).

Laboratory analyzes of the patina and encrustations provided the main operational indications to the restoration technicians for cleaning: these phenomena are mainly attributable to the photochemical smog and to the use of protective organic products, which, with time, have degraded. The films are often decayed and discontinuous, presenting colors from pale pink to yellow, to ochre or brown.

Regarding the identification of the compounds forming the patina, almost identical qualitative results were obtained for all samples analyzed (Figure 5). FT-IR spectra exhibited typical vibration bands of calcium sulphate hydrate, commonly called gypsum ($CaSO_4 \cdot 2H_2O$), centered at 1109, 669, and 596 cm^{-1}, as well as the stretching and deformation vibrations of the O-H bond of water at 3525, 3492, 3401 cm^{-1}, and at 1692 and 1627 cm^{-1}, respectively. In several analyzed samples, a representative band of silicates was present at 1036 and 1006 cm^{-1} (Si-O stretching vibrations). Gypsum originates from the transformation of calcite in the presence of sulphur oxides, while silicate was subsequently embedded in the crust due to the deposition of wind-borne particles.

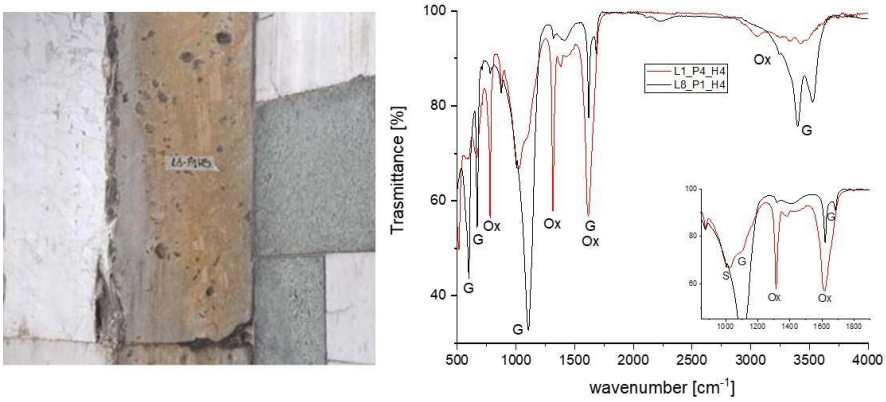

Figure 5. Photographic documentation of yellow-brown patinas on marble cladding. FT-IR spectra of two analyzed patinas, samples L1_P4_H4 and L8_P1_H5: G, gypsum; Ox, calcium oxalate; S, silicate.

Most notably, the prominent bands of calcium oxalate ($CaC_2O_4 \cdot nH_2O$) at 1324 (and 780 cm^{-1} were present. The features determined in the spectra suggested the presence of the mineralogical phase of calcium oxalate monohydrate, whewellite ($CaC_2O_4 \cdot H_2O$) (Figure 5). This identification was due to the presence of very specific bands at 3487, 3435, 3341, and 3068 (O-H stretching bands), 1624 and 1324 (C=O stretching vibration), and 780 and 674 cm^{-1} (O-C-O bending vibrations).

Calcium oxalate films are very stable, less soluble, and hardly affected by atmospheric pollution. Wherever the patinas, sometimes caused problematic removal, are discontinuous, especially near the friezes and decorative modules, the underlying marble appears detached, and a sugar-like crumbling can be observed.

In several darker patinas, the presence of organic matter in the FT-IR spectra was highlighted exclusively by the weak bands at 2916 cm^{-1} and 2841 cm^{-1} (Figure 6a,b), attributed to the stretching asymmetric and symmetric vibrations, respectively, of methyl and methylene groups, the bands in the region (1470–1375 cm^{-1}) due to CH_2 bending vibrations, and the methylene group rocking vibrations near 720 cm^{-1}. Figure 6b shows typical vibrations of the microcrystalline wax used as a protective treatment employed in the previous restorations.

These patinas can be attributed to not only the remains of old protective treatments, but also to substances applied to adjust the color of new marble elements to those which are older. This is the case of the sample in Figure 7, where the Raman analysis shows the presence of a yellow brownish pigment, yellow ochre (iron oxides and hydroxides), calcite (1086 cm^{-1}), gypsum (1007 cm^{-1}), and calcium sulphate (1019 cm^{-1}). The results suggest that the yellow patina is linked to a previous maintenance intervention of color toning of the window frame: in fact, it is assumed that it has been given a coating with lime water and yellow ochre.

Previous research, consisting of a multi-analytical approach for the study of the presence of red discouloration on the white marble of the external cladding of the Bapstistery, pointed out that the red staining is due to the presence of minium (lead tetraoxide) concentrated prevalently in the calcite crystal boundaries [26].

3.2. Marbles

In the Table 2 the mineralogical, petrographic, and isotopic features of white and veined marbles are reported.

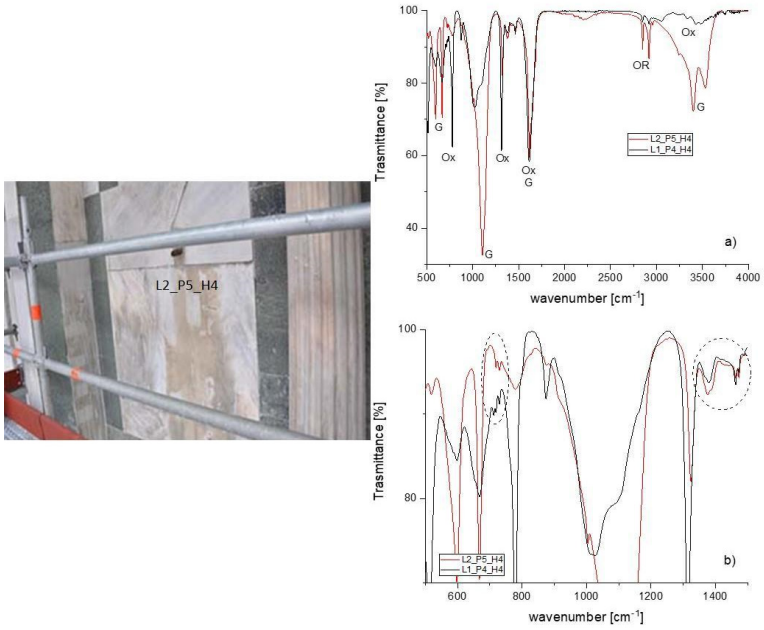

Figure 6. Photographic documentation of dark brown patinas on marble. FTIR spectra of two samples are reported showing the presence of: (**a**) Ox, calcium oxalate; G, gypsum; OR, organic compound, microcrystalline wax. (**b**) Detail of the spectra between 500 to 1500 cm^{-1}: the dashed circles highlight the vibrational bands of microcrystalline wax.

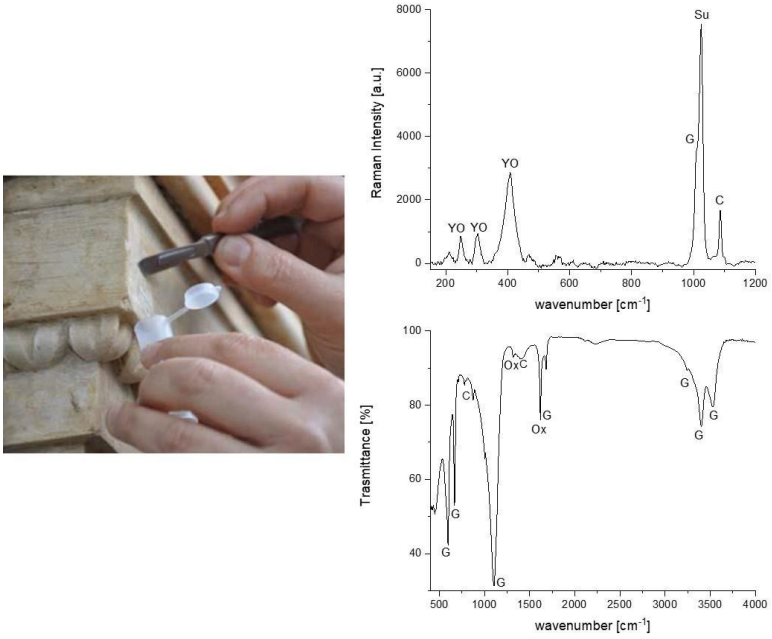

Figure 7. Raman and FT-IR spectra of the yellow-brownish patina: YO, yellow ochre; G, gypsum; Su, calcium sulphate; C, calcite; Ox, calcium oxalate.

Table 2. Summary of the main minero-petrographic and isotopic features of analyzed marble samples.

Id Sample	Position	Mineralogical Composition	MGS	Type of Fabric	Main Features of Microstructure	Grain Boundaries	$\delta^{13}C$	$\delta^{18}O$	Provenance
M1	Side 6	Calcite	1 mm	HE	Mosaic, lineated with deformed crystals	Curved	3.35	−2.56	Hymettus
M2	Side 6	Calcite, quartz *	650 μm	HO	Mosaic	Curved	1.46	−5.19	Lasa
M3	Side 6	Calcite, quartz *	800 μm	HE	Mosaic, lineated	Straight/curved	-	-	Uncertain attribution
M4	Side 6	Calcite	350 μm	HO	Mosaic, polygonal	Straight	-	-	Carrara
M5	Side 2	Calcite	1.5 mm	HE	Mosaic, fine-grained areas and strained crystals	Curved	2.77	−0.46	Greek marble (Paros II)
M6	Side 8	Calcite	400 μm	HO	Mosaic, polygonal	Straight	-	-	Carrara
M7	Side 8	Calcite, mica *, quartz *	550 μm	HE	Mortar, lineated	Straight/curved	-	-	Uncertain attribution
M8	Side 6	Calcite, quartz *	150 μm	HO	Mosaic, polygonal	Straight	1.63	−3.25	Carrara
M9	Side 7	Calcite	500 μm	HO	Mosaic, polygonal	Straight	2.01	−1.73	Carrara
M10	Side 8	Calcite, mica *, quartz *	550 μm	HE	Mosaic	Straight/curved	1.32	−7.77	Pentelicum
M11	Side 9	Calcite, dolomite, mica *, quartz *	550 μm	HE	Mosaic	Straight/curved	0.15	−6.56	Pentelicum
M12	Side 4	Calcite, mica *, quartz *	350 μm	HO	Mosaic, polygonal	Straight	2.10	−1.51	Carrara
M13	Side 4	Calcite, quartz *	350 μm	HO	Mosaic, polygonal	Straight	2.15	−1.67	Carrara
M14	Side 3	Calcite, dolomite *, quartz *	1 mm	HE	Lineated	Curved/embayed	1.81	−8.12	Pentelicum
M15	Side 2	Calcite, quartz *	500 μm	HO	Mosaic, polygonal	Straight	2.00	−1.51	Carrara
M16	Side 2	Calcite, quartz *	350 μm	HO	Mosaic, polygonal	Straight	2.10	−1.51	Carrara
M17	Side 2	Calcite, mica *, quartz *	500 μm	HO	Mosaic, polygonal	Straight	2.15	−1.67	Carrara
M18	Side 6	Calcite, mica *, quartz *	500 μm	HO	Mosaic, polygonal	Straight	2.35	−1.16	Carrara
M19	Side 6	Calcite, mica *, dolomite *, quartz *	500 μm	HO	Mosaic, polygonal	Straight	2.11	−1.76	Carrara

Table 2. *Cont.*

Id Sample	Position	Mineralogical Composition	MGS	Type of Fabric	Main Features of Microstructure	Grain Boundaries	$\delta^{13}C$	$\delta^{18}O$	Provenance
M20	Side 4	Calcite, Kfeld *, quartz *	1.5 mm	HE	Mortar	Straight/curved	3.07	−1.97	Hymettus
M21	Side 1	Calcite, dolomite, mica *, quartz *	2 mm	HE	Mortar, with deformed crystals	Curved/sutured	2.33	−3.15	Hymettus
M22	Side 6	Calcite, quartz *	500 μm	HO	Mosaic, polygonal	Straight	2.07	−2.22	Carrara
M23	Side 4	Calcite, quartz *	500 μm	HO	Mosaic, polygonal	Straight	2.00	−2.08	Carrara
M24	Side 4	Calcite, dolomite *, quartz *	500 μm	HO	Mosaic, polygonal	Straight	2.21	−2.02	Carrara
M25	Side 9	Calcite, dolomite *, quartz *	2 mm	HE	Mortar, bimodal distribution	Curved/sutured	4.16	−1.60	Thassos/ Proconneso
M26	Side 6	Calcite, dolomite *, mica *	600 μm	HE	Lineated	Curved/embayed	2.61	−7.23	Pentelicum
M27	Side 3	Calcite, mica *	700 μm	HE	Lineated	Curved/embayed	2.54	−7.03	Pentelicum

* Accessory minerals; MGS = maximum grain size; HO: homeoblastic; HE: heteroblastic.

Only a multi-analytical approach allows us to identify, with good probability, the origin of a marble: the minero-petrographic analyzes of thin sections and the data from the stable C and O isotope ratio are the most consolidated methods [6,27–32].

Mineralogical and petrographic characteristics (microstructure, significant accessory minerals, maximum grain size (MGS) and boundary types of the calcite and/or dolomite crystals) are related to the provenance of marbles, since they are related to the type and degree of metamorphism undergone by the original sedimentary protolith. A first general fabric classification is based upon the equal or different dimensions of the calcite or dolomite crystals, referred to as homeoblastic (HO) or heteroblastic (HE) classification, respectively. The grain size is connected with the metamorphic grade and the MGS (maximum grain size) is reported in the most used database as one of the most diagnostic parameters. Moreover, the shape of the calcite or dolomite crystal boundaries reflects the blastesis/deformation relationships during a tectono-metamorphic event that generated marble crystallization [7,8].

The isotopic ratios of C and O are related to the primary genetic (sedimentation) and evolutionary (diagenesis-metamorphism) processes that have affected the formation of marbles [33].

Combining minero-petrographic features and isotopic data (Table 2), different provenance for marbles used in the San Giovanni Baptistery can be identified:

- Carrara marble (Italy), white and veined, with a typical homeoblastic fabric, a mosaic-polygonal microstructure, with straight grain boundaries, MGS ranging from 150 to 500 micron, and isotopic ratios of C from 1.63 to 2.35 and O from −3.25 to −1.16, is used in the original and substituted portions of monument (Figure 8a,b);
- Hymettus marble (Greece), likely coming from the spolia of Fiesole Roman Theatre, Capitolium, and Thermae [9] is a white bluish marble characterized by grey/blue veins. The fabric is heteroblastic, with mosaic, lineated microstructure, curved grain boundaries, and an MGS ranging from 1 mm and 2 mm. The isotopic ratio varies from 3.35 to 2.33 for C and from −3.15 to −1.97 for O (Figure 8c,d);
- Lasa marble, used in the 20th century for the substitution of the most weathered slabs, comes from Laas (Lasa, South Tyrol, Northern Italy), and was selected by restorers for the macroscopic similarities to Hymettus marble (Figure 8e) [34]. It is a pure calcitic marble, containing small amounts of quartz, with a homeoblastic fabric and mosaic microstructure. The grain boundaries are prevalently curved (Figure 8f). The isotopic ratios of C and O fall in the range of data published on Lasa marbles [35];
- Other ancient marbles are most probably re-used marbles (i.e., Paros, Pentelicum) for some decorative elements (Figure 4).

Some uncertainties remain for some samples due to insufficient material available to perform all of the necessary analyzes. In fact, for M3 and M7 samples, obtaining uncontaminated powders for isotopic analyzes was impossible.

The analytical data obtained on provenance of marbles were used to upgrade the database of materials presented in [9,36].

3.3. Mortars

The main mineralogical and petrographic characteristics of analyzed samples are summarized in Tables 3 and 4, respectively. The analyzed mortar samples belong to: attic, S1, S2, S3, and S4; women's gallery, S5, and several masonry of basements, from S6 to S17 (summarized in Table 3).

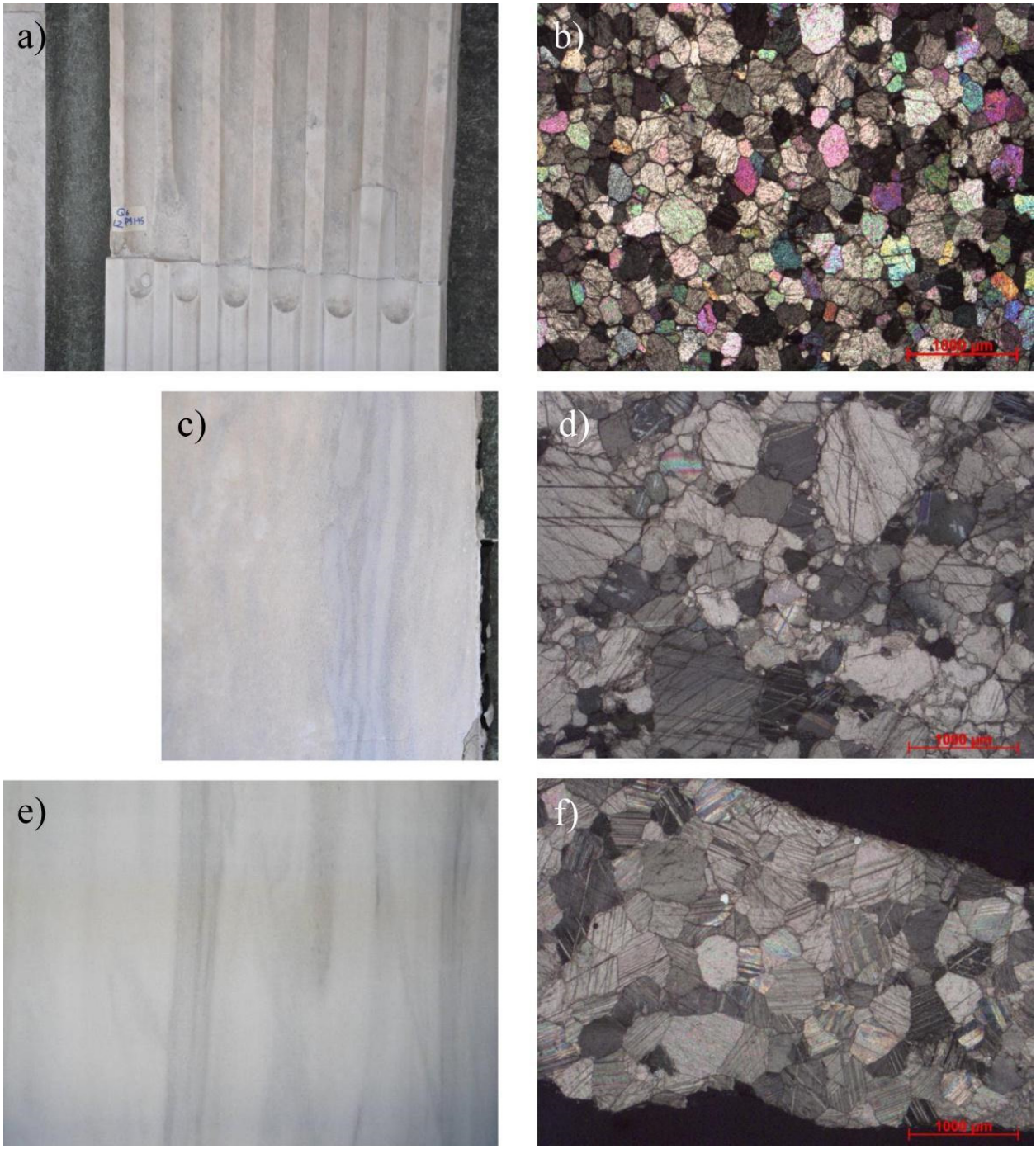

Figure 8. Macroscopic appearance and microphotograph of thin sections of marbles (by polarized optical microscopy; crossed nicols) of external cladding of the Baptistery (**a**,**b**) Cararra; (**c**,**d**) Hymettus; (**e**,**f**) Lasa.

Table 3. Mineralogical composition (semiquantitative data) of mortars.

Mortar Samples	Position	Depth	Quartz	Calcite	Plagioclase	K Feldspar	Other
S1	Attic, side 10	10–15 cm	+++	+	+	-	Muscovite (*), chlorite (*)
S2	Attic, side 10	9–14 cm	+++	++	+	+	Muscovite (+), chlorite (*)
S3	Attic, side 4–5	9–25 cm	+++	+	+	+	Muscovite (*), chlorite (*)
		25–30 cm	+++	+	+	+	Muscovite (*), chlorite (*)
S4	Attic, side 4	4–20 cm	+++	+	+	-	Muscovite (*), chlorite (*)
		20–35 cm	+++	++	++	*	Muscovite (*), chlorite (*), portlandite (*)
S5	Women's gallery, side 1	7–12 cm	+++	++	+	+	Muscovite (+), chlorite (*)
		12–26 cm	+++	++	+	+	Muscovite (*), chlorite (*)
		26–38 cm	+++	++	++	+	Muscovite (*), chlorite (*)
S6	Basements, side 9–10	0–10 cm	++	+++	+	-	Muscovite (*)
		10–32 cm	+++	++	*	-	Muscovite (*)
S7	Basements, side 9–10	0–11 cm	+++	++	*	*	Muscovite (*), chlorite (*), vaterite (*)
		11–32 cm	+++	+	+	-	Muscovite (*), chlorite (*), gypsum (*)
S8	Basements, side 8	0–12 cm	+++	++	++	+	Muscovite (+), chlorite (*)
		12–38 cm	+++	+	+	*	Muscovite (*), chlorite (*)
S9	Basements, side 9	0–11 cm	+++	+	*	-	Muscovite (*)
		11–21 cm	+++	+	+	+	Muscovite (*), chlorite (*)
		21–38 cm	+++	++	+	-	Muscovite (*), chlorite (*)
S10	Basements, side 9–10	0–15 cm	+++	++	*	-	Muscovite (*)
		15–38 cm	+++	++	*	*	Muscovite (*)
S11	Basements, side 9	0–5 cm	+++	++	+	+	Muscovite (*)
S12	Basements, central part	0–4 cm	+++	++	+	+	Muscovite (*), vaterite (+)
S13	Basements, central part	0–5 cm	+++	+	+	-	Muscovite (*), chlorite (*), gypsum (*), vaterite (+)
S14	Basements, central part	0–4 cm	+++	++	+	*	Muscovite (*), chlorite (*)
S15	Basements, central part	0–2 cm	+++	++	+	*	Muscovite (*), chlorite (*)
S16	Basements, side 7	4–12 cm	+++	+	*	-	Muscovite (*)
S17	Basements, side 6	0–2 cm	+++	+	+	+	Muscovite (*), chlorite (*)

+++: very abundant; ++: abundant; +: present; *: traces; -: below detection limit.

Table 4. Petrographic description of core samples (B/A = binder/aggregate ratio).

Mortar Samples	Depth	Binder	Aggregate	B/A	Macroporosity
S1	S1 (10–15) cm	Natural hydraulic lime and heterogeneous structure and micritic/microsparitic texture. Numerous lumps	Composition: quartz (monocrystalline), feldspar, rock fragments (quartzite, sandstone, calcarenite, micritic limestone) and few *cocciopesto* grains Homogeneous grain size distribution Grain size: 100 μm–700 μm Shape: sub rounded	1/3–1/4	Medium amount due to pores of irregular shape

Table 4. *Cont.*

Mortar Samples	Depth	Binder	Aggregate	B/A	Macroporosity
S2	S2 (9–14) cm	Natural hydraulic lime and heterogeneous structure and micritic/microsparitic texture. Recrystallized binder. Numerous lumps	Composition: quartz (monocrystalline), feldspar, calcite, rock fragments (quartzite, sandstone, calcarenite, micritic limestone) Homogeneous grain size distribution Grain size 100 μm–>1 mm Shape: sub angular/sub rounded	1/3–1/4	Medium amount due to pores of irregular shape
S3	S3 (9–25) cm	Natural hydraulic lime and homogeneous structure and micritic texture. Some lumps	Composition: quartz (monocrystalline), feldspar, calcite, quartzite, few carbonates rock fragments and *cocciopesto* Homogeneous grain size distribution Mean grain size 150–200 μm, few mm grains Shape: sub angular	1/3	Medium amount due to pores elongated and sub rounded shape
	S3 (25–30) cm	Natural hydraulic lime and homogeneous structure and micritic texture. Numerous lumps	Composition: quartz (monocrystalline), feldspar, rock fragments (quartzite, calcarenite, micritic limestone, flint) and few cocciopesto grains Homogeneous grain size distribution Grain size 100 μm–>1 mm Shape: sub angular	1/3	Medium amount due to pores of sub rounded shape
S4	S4 (4–20) cm	Natural hydraulic lime and heterogeneous structure and micritic/microsparitic texture. Slight recrystallized binder Some lumps	Composition: quartz (monocrystalline), feldspar, rock fragments (quartzite, sandstone, calcarenite, micritic limestone) and few *cocciopesto* grains Homogeneous grain size distribution Grain size: 100 μm–700 μm Shape: sub angular	1/3	Medium amount due to microcracks and pores of sub rounded shape
	S4 (20–35) cm	Natural hydraulic lime and heterogeneous structure and micritic/microsparitic texture. Recrystallized binder Some lumps	Composition: quartz (monocrystalline), feldspar, rock fragments (quartzite, sandstone, calcarenite, micritic limestone) and few *cocciopesto* grains Homogeneous grain size distribution Grain size 100 μm–1 mm Shape: sub angular/sub rounded	1/2–1/3	Medium/high amount due to pores of irregular and sub rounded shape

Table 4. *Cont.*

Mortar Samples	Depth	Binder	Aggregate	B/A	Macroporosity
S5	S5 (7–12) cm	Natural hydraulic lime and heterogeneous structure and micritic/microsparitic texture. Recrystallized binder. Numerous lumps	Composition: quartz (monocrystalline), feldspar, rock fragments (quartzite, sandstone, micritic limestone) Heterogeneous grain size distribution Grain size 100 μm–600 μm Shape: sub angular/sub rounded	1/3	Medium amount due to microcracks and pores of irregular shape
	S5 (12–26) cm	Natural hydraulic lime and heterogeneous structure and micritic texture. Recrystallized binder. Numerous lumps	Composition: quartz (monocrystalline), feldspar, several fragments of carbonate rocks and quartzite, sandstone rocks Homogeneous grain size distribution Grain size 100 μm–600 μm Shape: sub angular/ sub rounded	1/2–1/3	Medium amount due to pores of irregular and sub rounded shape
	S5 (26–38) cm	Natural hydraulic lime and heterogeneous structure and micritic/microsparitic texture. Recrystallized binder. Numerous lumps	Composition: quartz (monocrystalline), feldspar, rock fragments (quartzite, calcarenite, micritic limestone, marble) and few *cocciopesto* grains Homogeneous grain size distribution Grain size 100 μm–600 μm Shape: sub angular/sub rounded	1/2–1/3	Medium amount due to microcracks and pores of sub rounded and irregular shape
S6	S6 (0–10) cm	Natural hydraulic lime and heterogeneous structure and micritic/microsparitic texture. Recrystallized binder. Some lumps	Composition: quartz (monocrystalline), feldspar, abundant fragments of carbonate rocks Homogeneous grain size distribution Grain size 100 μm–1 mm Shape: sub angular/sub rounded	1/3–1/4	High amount due to pores of irregular
	S6 (10–32) cm	Natural hydraulic lime and heterogeneous structure and micritic/microsparitic texture. Recrystallized binder. Some lumps	Composition: quartz (monocrystalline), feldspar, abundant fragments of carbonate rocks Homogeneous grain size distribution Grain size 100 μm–1 mm Shape: sub angular/sub rounded	1/3–1/4	High amount due to pores of irregular shape

Table 4. *Cont.*

Mortar Samples	Depth	Binder	Aggregate	B/A	Macroporosity
S7	S7 (0–11) cm	Natural hydraulic lime and heterogeneous structure and micritic/microsparitic texture. Recrystallized binder. Some lumps	Composition: quartz (monocrystalline), feldspar, rock fragments (micritic limestone, flint, quartzite, calcarenite) Homogeneous grain size distribution Grain size 100 μm–1 mm Shape: sub angular/sub rounded	1/3–1/4	High amount due to pores of irregular shape
	S7 (11–32) cm	Natural hydraulic lime and heterogeneous structure and micritic/microsparitic texture. Some lumps.	Composition: quartz (monocrystalline), feldspar, abundant fragments of carbonate rocks, fragments of sandstone Homogeneous grain size distribution Grain size 100 μm–1 mm Shape: sub angular/sub rounded	1/3–1/4	High amount due to pores of irregular shape
S8	S8 (0–12) cm	Natural hydraulic lime and heterogeneous structure and micritic/microsparitic texture. Recrystallized binder. Some lumps	Composition: quartz (monocrystalline), feldspar, quartzite, few fragments of carbonate rocks and flint Homogeneous grain size distribution Grain size 100 μm–1 mm Shape: sub angular/sub rounded	1/4	Medium/ high amount due to pores of irregular shape
	S8 (12–38) cm	Natural hydraulic lime and heterogeneous structure and micritic/microsparitic texture. Numerous lumps	Composition: quartz (monocrystalline), feldspar, quartzite, few fragments of carbonate rocks Homogeneous grain size distribution Grain size 100 μm–1 mm Shape: sub angular/sub rounded	1/3–1/4	Low amount due to pores of irregular shape
S9	S9 (0–11) cm	Natural hydraulic lime and heterogeneous structure and micritic/microsparitic texture. Recrystallized binder. Some lumps	Composition: quartz (monocrystalline), feldspar, mica, quartzite, few fragments of carbonate rocks Homogeneous grain size distribution Grain size 100 μm–500 μm Shape: sub angular/sub rounded	1/3–1/4	High amount due to pores of irregular shape
	S9 (11–21) cm	Natural hydraulic lime and heterogeneous structure and micritic/microsparitic texture. Recrystallized binder. Some lumps	Composition: quartz (monocrystalline), feldspar, mica, quartzite, few fragments of carbonate rocks and *cocciopesto* Homogeneous grain size distribution Grain size 100 μm–700 μm Shape: sub angular/sub rounded	1/3–1/4	High amount due to pores of irregular shape

Table 4. *Cont.*

Mortar Samples	Depth	Binder	Aggregate	B/A	Macroporosity
	S9 (21–38) cm	Natural hydraulic lime and heterogeneous structure and micritic/microsparitic texture. Recrystallized binder. Some lumps	Composition: quartz (monocrystalline), feldspar, mica, quartzite, few fragments of carbonate rocks (with fossil, calcarenite) Homogeneous grain size distribution Grain size 100 μm–500 μm Shape: sub angular/sub rounded	1/3	High amount due to pores of irregular shape
S10	S10 (0–15) cm	Natural hydraulic lime and heterogeneous structure and micritic/microsparitic texture. Recrystallized binder. Some lumps	Composition: quartz (monocrystalline), feldspar, mica, quartzite, large and abundant fragments of carbonate rocks (with fossil, calcarenite) Heterogeneous grain size distribution Grain size 100 μm–700 μm Shape: sub angular	1/3	High amount due to pores of irregular shape
	S10 (15–38) cm	Natural hydraulic lime and heterogeneous structure and micritic/microsparitic texture. Recrystallized binder. Few lumps	Composition: quartz (monocrystalline), feldspar, mica, quartzite, calcite, abundant fragments of carbonate rocks (with fossil, calcarenite) and fragments of *cocciopesto* Heterogeneous grain size distribution Grain size 100 μm–700 μm Shape: sub angular	1/3	High amount due to pores of irregular shape
S11	S11 (0–21) cm	Natural hydraulic lime and heterogeneous structure and micritic/microsparitic texture. Recrystallized binder. Few lumps	Composition: quartz (monocrystalline), feldspar, quartzite, flint, calcite, abundant fragments of carbonate rocks (with fossil, calcarenite) and fragments of *cocciopesto* Homogeneous grain size distribution Grain size 100 μm–800 μm Shape: sub angular	1/3–1/4	High amount due to pores of irregular shape
S12		Lime hydraulicized with crushed ceramics and heterogeneous structure and micritic/microsparitic texture. Recrystallized binder. Absent lumps	Composition: cocciopesto, calcite, carbonate fragments and some fragments of sandstone, abundant fragments of carbonate rocks Heterogeneous grain size distribution (bimodal) Grain size 50 μm–1 mm Shape: sub angular/sub rounded	1/2–1/3	Medium amount due to pores of irregular shape

Table 4. *Cont.*

Mortar Samples	Depth	Binder	Aggregate	B/A	Macroporosity
S13		Natural hydraulic lime and homogeneous structure and microsparitic texture. Recrystallized binder. Some lumps	Composition: quartz (monocrystalline), feldspar, rock fragments (micritic limestone, quartzite) and few fragments of *cocciopesto* Heterogeneous grain size distribution Grain size 100 μm–800 μm Shape: sub angular	1/2	High amount due to pores of irregular shape
S14		Natural hydraulic lime and homogeneous structure and micritic texture. Some lumps	Composition: quartz (monocrystalline), feldspar, sandstone few fragments of carbonate and rare fragments of *cocciopesto* Homogeneous grain size distribution Grain size 100 μm–500 μm Shape: sub angular	1/1–1/2	Medium amount due to pores of irregular shape
S15		Natural hydraulic lime and heterogeneous structure and micritic/microsparitic texture. Recrystallized binder. Some lumps	Composition: quartz (monocrystalline), feldspar, few fragments of carbonate rocks and *cocciopesto* Homogeneous grain size distribution Grain size 100 μm–500 μm Shape: sub angular/sub rounded	1/3	High amount due to pores of irregular shape
S16		Natural hydraulic lime and heterogeneous structure and micritic/microsparitic texture. Recrystallized binder. Some lumps	Composition: quartz (monocrystalline), feldspar, fragments of sandstone, few fragments of carbonate rocks and *cocciopesto* Homogeneous grain size distribution Grain size 100 μm–500 μm Shape: sub angular	1/3–1/4	Medium amount due to pores of irregular shape
S17		Natural hydraulic lime and heterogeneous structure and micritic/microsparitic texture. Some lumps	Composition: quartz (monocrystalline), feldspar, few fragments of carbonate rocks and *cocciopesto* Homogeneous grain size distribution Grain size 100 μm–800 μm Shape: sub angular	1/3	High amount due to pores of irregular shape

The mineralogical analysis indicates the presence of quartz, calcite, plagioclase, and micas in all samples. Calcite refers to the binder and aggregate fractions; this is due to the presence, in the aggregate, of carbonate fragments of rocks, such as micritic limestone, marly limestone, and single calcite crystals. Semi-quantitative results indicate the presence prevailing of quartz, feldspars (plagioclase and K feldspar), and minor amounts of phyllosilicates (mica-like minerals and chlorites), referred to as the aggregate composition. K feldspars are not present only in the samples S1, S4, S6, S7 (deepest sample), S9 (except in intermediate depth sample), S10 (most superficial sample), S13, and S16; while chlorite is not present in the samples S6, S9 (most superficial sample) S10, S11, S12, and S16. A calcium carbonate polymorphous, vaterite, was individuated in samples S7 (most

superficial sample), S12, and S13. Vaterite was typically found in the Florentine mortars, associated with the production of natural hydraulic binders obtained by burning marly limestone [17,19,37]. The presence of portlandite ($Ca(OH)_2$) in the deepest sample of S4 was noted, linked to an incomplete carbonation of binder. Gypsum was registered only in S13, belonging to the basement, most probably due to the sulphation phenomena of the binder.

The petrographic observation (Table 4) performed on Baptistery mortar samples shows, mainly, a binder with a heterogeneous structure and micritic/microsparitic texture, as well as the presence of lumps, both as remnants of the binder not being well mixed and as remnants of overburnt limestone fragments. An exception is represented by S12 sample, which came from the basement, collected from the mosaic masonry, composed of lime hydraulicized with crushed ceramics.

In some cases, the binder of the mortars was subjected to processes of dissolution and recrystallization by aqueous solutions circulating in the masonry, and occurred inside the pore space. The recrystallizations are present in the majority of samples, except in S1, S3, S14, S17, and in the internal samples S5, S7, and S8. Often, the absence of dissolution and recrystallization phenomena is correlated to the homogeneous characteristic of the binder, as shown in samples S3 and S14. The aggregate is, on average, abundant, mainly with homogeneous distribution (except in S5, which is the most superficial sample, and S10, S12, S13, which present heterogeneous grain size distribution) and well selected grain size composed of quartz, feldspars, mica, calcite, and fragments of carbonate rocks.

The core samples extracted from the attic, samples S1, S2, S3, and S4, were obtained by mixing a natural hydraulic binder with an abundant aggregate (B/A 1/3–1/4), characterized by numerous lumps (Figure 9a) and heterogeneous structure and micritic/microsparitic texture (Figure 9b), with the exception of S3, which presents homogeneous structure and micritic texture (Figure 9c), and S4, which is composed by lower B/A, equal to 1/2–1/3. Lumps observed in the binder are useful for identifying the limestone burnt to obtain lime, which appears in the local Alberese limestone (Figure 9a). The aggregate has a homogeneous grain size distribution, ranging from 1 mm for rock fragments to 100 μm for monocrystals. Quartz, plagioclases, rock fragments (quartzite, sandstones, calcarenite, micritic limestone), and few *cocciopesto* fragments were identified under optical microscopy. The aggregate shape is sub angular, and a medium macroporosity due to pores of irregular shape was observed. In S4 (20–35 cm), the macroporosity is more developed (medium-high) and characterized by a recrystallized binder. Some differences in samples belonging to different core depths have been classified by grain size distribution and composition of aggregate, but the production of the binder has been the same.

For core sample S5, which was obtained from the women's gallery, three samples extracted from different depths were investigated. Mortars were realized with a natural hydraulic binder, numerous lumps referred to the binder being not well mixed, and remnants of overburnt marly limestones, identified as the local Alberese limestone, were observed (Figure 9d). All mortar samples suffered a strong recrystallization of the binder in the form of spathic calcite. In different depths of S5, some differences in the aggregate characteristics were present: S5 (7–12) cm was composed of abundant binder/aggregate (B/A 1/3) and fine grain size predominant, while S5 (12–26) cm and S5 (26–38) cm were characterized by less binder/aggregate (B/A 1/2–1/3), and a fine-medium size was predominant (Figure 9e). Furthermore, a different amount of carbonate rock fragment was registered, with respect to the attic mortar samples (a higher entity in S5 samples).

For samples S6 to S17, belonging to the basement of the Baptistery, a binder made with natural hydraulic lime with a heterogeneous structure and micritic/microsparitic texture were observed. They show some differences: the binder of the S13 sample has a microsparitic texture (Figure 9f), and S14 has micritic texture (Figure 9g), while the binder of remaining samples has a micritic/microsparitic aspect (Figure 9h). The binder of the major parts of samples are characterized by a relevant recrystallization and heterogeneous structure. Some differences have also been registered in grain size distribution and aggre-

gate composition for the same mortar core. A fair amount of carbonate rock fragments was registered, with abundant presence in S6, S10, S11, and S12 (S6 in Figure 9i). In the mortar basement samples, the aggregate has a homogeneous grain size distribution ranging from 800 μm^{-1} mm to 100 μm, and in S10 and S13 a heterogeneous grain size distribution was observed (grain size 800–100 μm). The aggregate shape is sub angular/sub rounded, with a high microporosity due to pores of irregular shape observed.

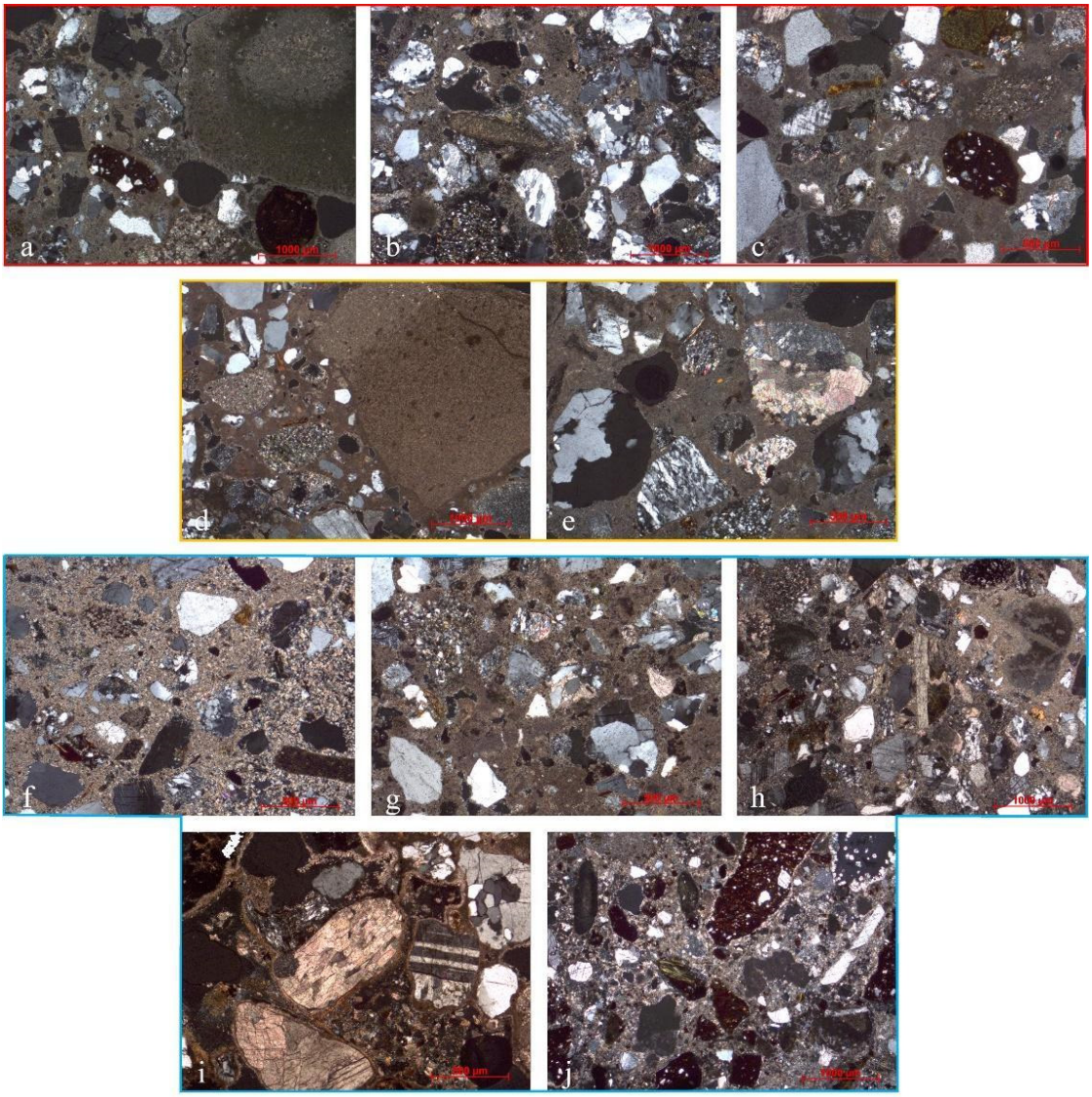

Figure 9. Microphotograph of thin sections of some selected mortar samples: (**a**) S1, (**b**) S2, (**c**) S3, (**d**) S5 (12–26) cm, (**e**) S5 (26–38) cm, (**f**) S13, (**g**) S14, (**h**) S7, (**i**) S6 and (**j**) S12 (by polarized optical microscopy; crossed nicols).

In sample S12, coming from the basement and collected from the mosaic masonry, crushed ceramic (or *cocciopesto*) was added to the mix consisting of air hardening calcitic lime and fine quartzitic/carbonate aggregate, and the ratio of B/A is 1/2–1/3. The crushed ceramics have a hydraulic function, because the original clay minerals, during firing, become amorphous, and may react with the lime (calcium hydroxide) to form hydrated calcium silicates and hydrated calcium aluminates [17]. Lime hydraulicized with crushed ceramics, a heterogeneous structure, a micritic/microsparitic texture, and an absence of lumps were observed (Figure 9j).

The TGA analyzes were performed on representative samples: the selection was based on petrographic observations. The samples from attic: S1 (10–15) cm, S2 (9–14) cm, S3 (0–4) cm, S4 (4–20) cm; from the women's gallery: S5 (7–12) cm, S5 (12–26) cm, S5 (26–38) cm; and from the basement S8 (21–38) cm, S12 (0–4) cm, S14 (0–4) cm, and S16 (4–12) cm were analyzed. The variation of hydraulic behavior in the depth were evaluated in samples collected from the women's gallery (S5). Figure 10 shows the plot of the percentage of weight loss attributed to CO_2, as well as the percentage of weight loss attributed to hydraulic water (CO_2/H_2O ratio), and % CO_2, the significant parameters for identifying the type of binder used in the mortar mixture [24]. The presence of hydraulic components is registered through weight loss in the 200–600 °C temperature range, indicated as hydraulic water (%), the values of which range from 3.82% to 8.11%. The parameter %CO_2 is observed through weight loss in the 600–900 °C temperature range, and these values vary between 18.77% and 26.50%, resulting a material with a hydraulic behavior. The samples extracted from the same area present consistent hydraulic water and %CO_2 values. TGA results show that the samples from the attic, women's gallery, and basements of the Baptistery fall in the typical cluster of hydraulic mortars, and are characterized by a rather homogeneous hydraulicity. In the same cluster, but away from the other samples, S12, has a different setting reaction of binder (setting and hardening both through carbonation of calcium hydroxide and through reaction of calcium hydroxide itself with the hydraulicizing components), which is present in petrographic observation [17]. The S5 samples (analyzed at three different depths) show small differences among samples selected at different depths, suggesting that there is a slight variation of hydraulic behavior. The TGA results confirm the hydraulic behavior, as suggested by the presence of lumps of unburnt Alberese limestone in petrographic observations. The firing of marly limestone provides natural hydraulic lime, typically produced in the Florentine area [19,37–39].

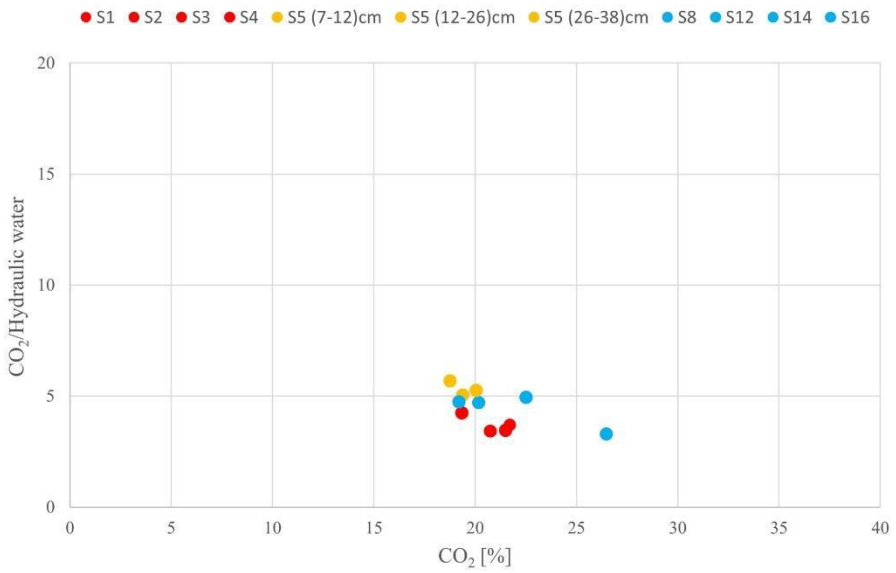

Figure 10. Plot of CO_2/H_2O ratio vs. %CO_2 measured on the enriched binders of mortar samples by TGA analysis.

Finally, the mortar samples show, mainly, the presence of lumps which are typical of Alberese limestone, suggesting the use of this stone to produce lime. Moreover, their presence in the mixtures testifies to traditional technologies. This raw material is able to confer to the mortar good performance, durability, and hydraulic behavior, as observed from the TGA results. Through the analysis of core samples at different depths, no substantial differences were found, and incomplete carbonation of the binder was observed in the deepest portion. The mortars of the Baptistery are composed of aggregate consisting of variable compositions (different amounts of monocrystals, carbonate, and silicate rock fragments)

and abundance (B/A ranges from 1/1–1/2 to 1/3–1/4). In attic and basement samples, a predominance of carbonate rock fragments was registered. The macroporosity was medium in the attic and women's gallery mortar samples, and high in the basement samples, due to pores of irregular shape. The high porosity and the position of basement mortars involve a binder characterized by a relevant recrystallization, as revealed in petrographic observations. The sample, collected from the mosaic masonry, is a hydraulic lime mortar used for the addition of *cocciopesto*. This artificial material, obtained by crushing bricks or ceramic, reacts with the air hardening lime binder, developing amorphous hydrated calcium silicates and hydrated calcium aluminates which are able to set under conditions of high humidity or under water, thereby allowing the preparation of mortars with good mechanical characteristics and durability [19,20]. In the past, *cocciopesto* was mainly used for the preparation of mortars with different functions (floors, plasters, tanks, aqueducts) when natural pozzolans were unavailable, and has also been found in the preparation of mosaic layers [40].

3.4. Bricks

The mineralogical and petrographic characteristics of the brick samples coming from side 4 of the inner dome are summarized in Table 5. XRPD data show the presence of quartz, calcite, and plagioclase in all of the examined samples; muscovite is identified in samples 1A and 1D, traces of diopside were identified in sample 1B, and K feldspar in sample 1A. All of the detected minerals can be ascribed to raw materials used for the production of bricks, with the exception of diopside, which can nucleate for the reaction between carbonates and clay materials [21,41,42]. The coexistence of this newly formed mineral and calcite is quite a common occurrence, although the latter is not stable at high temperatures. Its presence can be explained by considering a secondary recrystallization due to the movement of Ca-rich solutions in the walls.

Table 5. Mineralogical composition (semiquantitative data) and petrographic description of bricks.

Brick Samples	Groundmass	Framework	Macroporosity	XRD Data
1A	Low birefringence	Composition: quartz, micas, plagioclase and k feldspar Well sorted Grain size 150–300 μm Shape: sub rounded/sub angular	Low, presence inside the pores of recrystallization of calcite	Quartz +++ Calcite * Plagioclase + K feldspar * Muscovite *
1B	Low birefringence	Composition: quartz, micas and plagioclase Well sorted Grain size 150–300 μm Shape: sub angular	Low, presence inside the pores of recrystallization of calcite	Quartz +++ Calcite * Plagioclase + Diopside *
1C	Low birefringence	Composition: quartz, plagioclase, carbonate rock fragments Medium sorted Grain size 150–500 μm Shape: sub angular	Medium	Quartz +++ Calcite + Plagioclase +
1D	Low birefringence	Composition: quartz, micas, plagioclase, carbonate rock fragment Grain size distribution (bimodal) 150–200 μm 1–2 mm Shape: sub rounded/sub angular	Medium	Quartz +++ Calcite * Plagioclase + Muscovite *

+++: very abundant; ++: abundant; +: present; *: traces.

Concerning the petrographic characteristics, two typologies have been identified: the first one (samples 1A and 1B) is characterized by a red colored paste (Figure 11a). The groundmass has a low birefringent with a medium amount of framework (ratio groundmass/framework 1/2). The framework is composed of quartz, plagioclase, and K

feldspar. The maximum grain size of the framework's components is 300 µm, the texture is not oriented, and secondary recrystallization of calcite in macroporosity is observed. The second typology (samples 1C and 1D) has a light red colored paste, and more abundant framework (ratio groundmass/framework 1/3) made of quartz, micas, plagioclase, and carbonate rock fragments (micritic limestones) (Figure 11b). The framework is not well sorted and selected. A bimodal grain size distribution was observed for sample 1D. A medium macroporosity was registered.

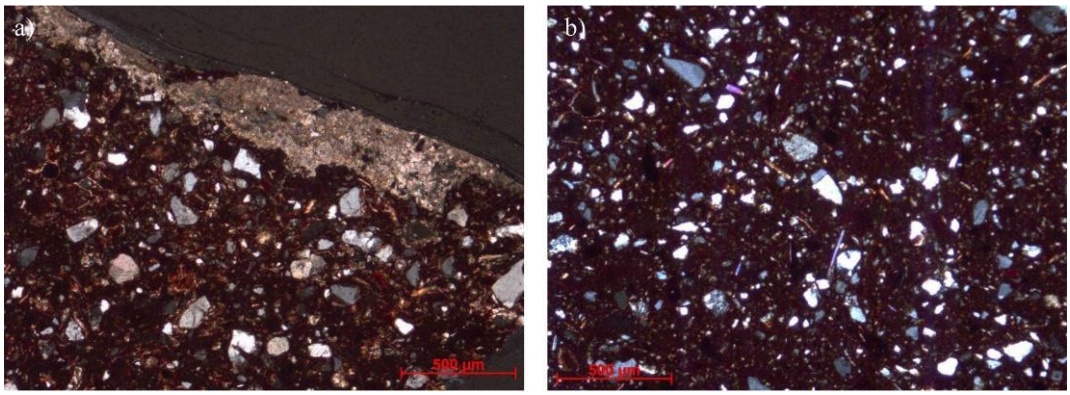

Figure 11. Microphotograph of thin sections of brick samples 1A and 1D, (**a**) and (**b**) respectively (through polarized optical microscopy; crossed nicols).

Thermoluminescence (TL) dating [14,43] of these samples revealed two different ages: 4th–5th century, and around the 20th century.

The first date is probably linked to the re-use of most ancient bricks, while the 20th century must be considered a post quem term for the building of the structure. The limited number of samples analyzed and dated cannot be considered exhaustive of the resolution of the chronological problematics in such a complex building.

A specific research project devoted to these materials would be desirable.

4. Conclusions

This research confirms the importance played by the mineralogical–petrographic and chemical characterisation of the stone materials utilized in historical architecture in order to understand their use, the role played in the urban development, and the durability towards atmospheric agents from the perspective of conservation. The results obtained represent a further milestone for better management of future restoration interventions, especially in terms of choosing of the best cleaning procedures for historical and monumental complexes.

To design the restoration interventions and maintenance of the Baptistery of San Giovanni, one of the most important churches in Florence (Italy) and protected by UNESCO since 1982, requires a complete characterization of the state of conservation and natural and artificial materials. The results are relevant for the knowledge of: (i) main phenomena of cladding alteration/decay, (ii) provenance of marbles, and (iii) the identification of raw materials and technologies used for their production of mortars and bricks.

The identification of altering processes in the materials provided the main operational indications to the restoration technicians for cleaning. The external surface presents patina and encrustations due to the photochemical smog, as well as the use of old protective treatments products which, with time, have degraded. The eight sides of the Baptistery have different states of conservation, both in terms of the characteristics of the materials, and of the different exposures to atmospheric agents. A conservative intervention aimed to remove the layers of black encrustations and the deposits of pollutants, as well as to consolidate the marble elements that have deteriorated over time, has been performed.

The different provenance of white and veined marble allows us to identify the construction phases, the restoration interventions, and the re-use of ancient materials. In this way, it was shown that the workshop originally used marble from Carrara (Carrara marble), and from Greece (Hymettus and Pentelicum marbles), the latter of which are most probably re-used marbles from the spolia of ancient buildings. After that, marble from Carrara and Laas (Lasa marble) were used for replacement interventions.

The mortars of the Baptistery consist of a natural hydraulic lime binder, obtained through the burning of a marly limestone, testified to be under-burnt fragments of Pietra Alberese (Monte Morello formation). This raw material is able to confer to the mortar good performance, durability, and hydraulic behavior, as observed from the TGA results. The aggregate is composed of silicate and carbonate components. Although all of the core samples were obtained from quite similar raw materials, different technological characteristics were observed: B/A ratio, sieving and mean grain size of aggregates, and macroporosity.

The two sets of brick samples, attributed to different ages (4th–5th and 20th century) through the thermoluminescence method, have different minero–petrographic features.

Supplementary Materials: The following supporting information can be downloaded at: https://www.mdpi.com/article/10.3390/app12084050/s1, Table S1: Main results, obtained with a multi-analytical approach, on state of conservation of external sides of San Giovanni Baptistery (Florence).

Author Contributions: Conceptualization, E.C., C.A.G. and B.A.; methodology, E.C. and S.V.; investigation, S.C., E.C., S.V. and M.R.; data curation, S.C., E.C., S.V. and M.R.; writing—original draft preparation, S.C., E.C., S.V. and M.R.; writing—review and editing, S.C., E.C., S.V. and M.R.; supervision, C.A.G. All authors have read and agreed to the published version of the manuscript.

Funding: This research did not receive any specific grant from funding agencies in the public, commercial, or not-for-profit sectors.

Institutional Review Board Statement: Not applicable.

Informed Consent Statement: Not applicable.

Data Availability Statement: Not applicable.

Acknowledgments: The authors are grateful to Opera del Duomo for giving them the opportunity to study the stone materials of the San Giovanni baptistery.

Conflicts of Interest: The authors declare no conflict of interest.

References

1. Morolli, G. L'architettura del Battistero e l'ordine antico. In *Il Battistero di San Giovanni*; Paolucci, A., Ed.; Franco Cosimo Panini: Modena, Italy, 1994; pp. 33–132.
2. Cardini, M. L'ipotesi tardo antica del Battistero. In *Il bel San Giovanni e Santa Maria del Fiore*; Cardini, D., Ed.; Le Lettere: Firenze, Italy, 1996; pp. 62–93.
3. Rocchi Coopmans de Yoldi, G. Il Battistero di San Giovanni: Lo svolgimento della fabbrica. In *Santa Maria del Fiore—Piazza, Battistero, Campanile*; Rocchi Coopmans de Yoldi, G., Ed.; Università Degli Studi di Firenze, Dipartimento di Architettura, Il Torchio: Firenze, Italy, 1996; pp. 27–72.
4. Degl'Innocenti, P. Misurare, disegnare, conoscere: Dai rilievi del San Giovanni alle ipotesi storico-costruttive. In *Il Battistero di San Giovanni, Conoscenza, Diagnostica, Conservazione*; Gurrieri, F., Ed.; Mandragora: Firenze, Italy, 2017; pp. 87–103.
5. Siegesmund, S.; Torok, A. Building stones. In *Stone in Architectures. Properties, Durability*; Siegesmund, E., Snethlage, R., Eds.; Springer: Berlin/Heidelberg, Germany; New York, NY, USA; Dordrecht, The Netherlands; London, UK, 2014.
6. Antonelli, F.; Lazzarini, L. An updated petrographic and isotopic reference database for white marbles used in antiquity. *Rend. Fis. Acc. Lincei* **2015**, *26*, 399–413. [CrossRef]
7. Moens, L.; Roos, P.; Rudder, J.D.; Paepe, P.D.; Hende, J.V.; Waelkens, M. A multi-method approach to the identification of white marbles used in antique artifacts. In *Classical Marble: Geochemistry, Technology, Trade*; Herz, N., Waelkens, M., Eds.; Kluwer Academic Publishers: Dordrecht, The Netherlands, 1988; pp. 243–250. [CrossRef]
8. Lazzarini, L. Archaeometric aspects of white and coloured marbles used in antiquity: The state of the art. *Per. Mineral.* **2004**, *73*, 113–125.

9. Coli, M.; Ciuffreda, A.L.; Donigaglia, T.; Bencaster, A.; Caciagli, S.; Agostini, B.; Iandelli, N. Saint John Baptistery in Florence (Italy): Studies for Conservation of the External Marble Cladding. *Appl. Sci.* **2021**, *11*, 6329. [CrossRef]
10. Fratini, F.; Rescic, S.; Pittaluga, D. Serpentinite and ophicalcite in the architecture of eastern Liguria and as decoration of Tuscan religious buildings. *Resour. Polic* **2022**, *75*, 102505. [CrossRef]
11. Pecchioni, E.; Magrini, D.; Cantisani, E.; Fratini, F.; Garzonio, C.A.; Nosengo, C.; Santo, A.P.; Vettori, S.A. Non-Invasive Approach for the Identification of "Red Marbles" from Santa Maria Del Fiore Cathedral (Firenze, Italy). *Int. J. Archit. Herit.* **2021**, *15*, 494–504. [CrossRef]
12. Pecchioni, E.; Cantisani, E.; Fratini, F. La città di Firenze: Un museo di litologia all'aperto. In *Il Museo di Storia Naturale dell'Università degli Studi di Firenze*; Le collezioni mineralogiche e litologiche; Firenze University Press: Firenze, Italy, 2012; Volume IV, pp. 245–269.
13. Malesani, P.; Pecchioni, E.; Cantisani, E.; Fratini, F. Geolithology and provenance of materials of some historical buildings and monuments in the centre of Florence (Italy). *Episodes* **2003**, *26*, 250–255. [CrossRef]
14. Garzonio, C.A.; Cantisani, E.; Coli, M.; Cuzman, O.; Del Luca, D.; Lubrito, C.; Ricci, M.; Vettori, S.; Sibilia, E. I materiali costitutivi del Battistero. In *Il Battistero di San Giovanni, Conoscenza, Diagnostica, Conservazione*; Gurrieri, F., Ed.; Mandragora: Firenze, Italy, 2017; pp. 179–191.
15. Elsen, J. Microscopy of historic mortars—A review. *Cem. Concr. Res.* **2006**, *36*, 1416–1424. [CrossRef]
16. Ingham, J.P. *Geomaterials under the Microscope. A Colour Guide*; CRC Press: London, UK, 2010.
17. Pecchioni, E.; Fratini, F.; Cantisani, E. *Atlas of the Ancient Mortars in Thin Section under Optical Microscope*, 2nd ed.; Nardini: Florence, Italy, 2020.
18. Reedy, C.L. *Thin-Section Petrography of Stone and Ceramic Cultural Materials*; Archetype Publications: London, UK, 2008; p. 256. ISBN 978-1-9049-8233-3.
19. Cantisani, E.; Fratini, F.; Pecchioni, E. Optical and Electronic Microscope for Minero-Petrographic and Microchemical Studies of Lime Binders of Ancient Mortars. *Minerals* **2022**, *12*, 41. [CrossRef]
20. Arizzi, A.; Cultrone, G. Mortars and plasters-how to characterize hydraulic mortars. *Archaeol. Anthropol. Sci.* **2021**, *13*, 2–22. [CrossRef]
21. Maggetti, M. Phase analysis and its significance for technology and origin. In *Archaeological Ceramics*; Olin, J.S., Franklin, A., Eds.; Smithsonian Institution Press: Washigton, DC, USA, 1982; pp. 121–133.
22. Pavía, S. The determination of brick provenance and technology using analytical techniques from the physical sciences. *Archaeometry* **2006**, *48*, 201–218. [CrossRef]
23. Moropoulou, A.; Bakolas, A.; Bisbikou, K. Characterization of ancient, byzantine and later historic mortars by thermal and X-ray diffraction techniques. *Thermochim. Acta* **1995**, *269–270*, 779–795. [CrossRef]
24. Bakolas, A.; Biscontin, G.; Contardi, V.; Franceschi, E.; Moropoulou, A.; Palazzi, D.; Zendri, E. Thermoanalytical research on traditional mortars in Venice. *Thermochim. Acta* **1995**, *269–270*, 817–828. [CrossRef]
25. Maravelaki-Kalaitzaki, P.; Bakolas, A.; Moropoulou, A. Physico-chemical study of Cretan ancient mortars. *Cem. Concr. Res.* **2003**, *33*, 651–661. [CrossRef]
26. Cantisani, E.; Cuzman, O.A.; Vettori, S.; Chelazzi, L.; Ciattini, S.; Ricci, M.; Garzonio, C.A. A multi-analytical approach for the study of red stains on heritage marble. *Analyst* **2019**, *144*, 2375–2386. [CrossRef]
27. Pensabene, P.; Antonelli, F.; Lazzarini, L.; Cancelliere, S. Provenance of marble sculptures and artifacts from the so-called Canopus and other buildings of "Villa Adriana" (Hadrian's villa—Tivoli, Italy). *J. Archaeol. Sci.* **2012**, *37*, 994–1005. [CrossRef]
28. Columbu, S.; Antonelli, F.; Lezzerini, M.; Miriello, D.; Adembri, B.; Blanco, A. Provenance of marbles used in the Heliocaminus Baths of Hadrian's Villa (Tivoli, Italy). *J. Archaeol. Sci.* **2014**, *49*, 332–342. [CrossRef]
29. Antonelli, F.; Columbu, S.; Lezzerini, M.; Miriello, D. Petrographic characterization and provenance determination of the white marbles used in the Roman sculptures of Forum Sempronii (Fossombrone, Marche, Italy). *Appl. Phys. A* **2014**, *115*, 1033–1040. [CrossRef]
30. Antonelli, F.; Lazzarini, L. The use of white marble in the central and upper adriatic between Greece and Rome: Hellenistic Stelae from the necropolis of Ancona (Italy). *Camb. Archaeol. J.* **2013**, *23*, 149–162. [CrossRef]
31. Attanasio, D.; Boschi, C.; Bracci, S.; Cantisani, E.; Paolucci, F. Provenance Studies of the Marble of Ancient Sculptures in the Tribune of the Uffizi Gallery, Florence. *Archaeometry* **2015**, *57*, 74–89. [CrossRef]
32. Attanasio, D.; Boschi, C.; Bracci, S.; Cantisani, E.; Paolucci, F. The Greek and Asiatic marbles of the Florentine Niobids. *J. Archaeol. Sci.* **2016**, *66*, 103–111. [CrossRef]
33. Attanasio, D.; Brilli, M.; Ogle, N. *The Isotopic Signatures of Classical Marbles*; L'erma di Bretschneider: Rome, Italy, 2006; p. 279.
34. Bianchini, P. I Paramenti esterni. I materiali, i restauri degli anni 1938–1944 e cenni sullo stato di conservazione attuale. In *Santa Maria del Fiore—Piazza, Battistero, Campanile*; Rocchi Coopmans de Yoldi, G., Ed.; Università Degli Studi di Firenze, Dipartimento di Architettura; Il Torchio: Firenze, Italy, 1996; pp. 97–98.
35. Unterwurzacher, M.; Obojes, U. White marble from Laas (Lasa), south Tyrol-its occurrence, use and petrographic-isotopical characterisation. *Austrian J. Earth Sci.* **2012**, *105*, 26–37.
36. Iandelli, N.; Coli, M.; Donigaglia, T.; Ciuffreda, A.L. An Unconventional Field Mapping Application: A Complete Opensource Workflow Solution Applied to Lithological Mapping of the Coatings of Cultural Heritage. *ISPRS Int. J. Geo. Inf.* **2021**, *10*, 357. [CrossRef]

37. Cantisani, E.; Calandra, S.; Barone, S.; Caciagli, S.; Fedi, M.; Garzonio, C.A.; Liccioli, L.; Salvadori, B.; Salvatici, T.; Vettori, S. The mortars of Giotto's Bell Tower (Florence, Italy): Raw materials and technologies. *Constr. Build. Mater* **2021**, *267*, 120801. [CrossRef]
38. Cantisani, E.; Falabella, A.; Fratini, F.; Pecchioni, E.; Vettori, S.; Antonelli, F.; Giamello, M.; Lezzerini, M. Production of the Roman Cement in Italy: Characterization of a raw material used in Tuscany between 19th and 20th century and its comparison with a commercialized French stone material. *Int. J. Archit. Herit.* **2018**, *12*, 1038–1050. [CrossRef]
39. Lezzerini, M.; Ramacciotti, M.; Cantini, F.; Fatighenti, B.; Antonelli, F.; Pecchioni, E.; Fratini, F.; Cantisani, E.; Giamello, M. Archaeometric study of natural hydraulic mortars: The case of the Late Roman Villa dell'Oratorio (Florence, Italy). *Archaeol. Anthrop. Sci.* **2017**, *9*, 603–615. [CrossRef]
40. Megna, B.; Rizzo, G.; Ercoli, L. The mortars and plasters under the mosaics and the wall paintings of the Roman villa at Piazza Armerina, Sicily. In Proceedings of the 2nd Conference on Historic Mortars—HMC 2010 and RILEM TC 203-RHM Final Workshop, Prague, Czech Republic, 22–24 September 2010; pp. 275–283.
41. Riccardi, M.P.; Messiga, B.; Duminuco, P. An approach to the dynamics of clay firing. *Appl. Clay Sci.* **1999**, *15*, 393–409. [CrossRef]
42. Cultrone, G.; Rodriguez-Navarro, C.; Sebastian, E.; Cazalla, O.; De la Torre, M.J. Carbonate and silicate phase reactions during ceramic firing. *Eur. J. Mineral.* **2001**, *13*, 621–634. [CrossRef]
43. Galli, A.; Martini, M.; Maspero, F.; Panzeri, L.; Sibilia, E. Surface dating of bricks, an application of luminescence techniques. *Eur. Phys. J. Plus* **2014**, *129*, 101. [CrossRef]